Journal of Sciences, Islamic Republic of Iran 26(4): 333 - 348 (2015) http://jsciences.ut.ac.ir
University of Tehran, ISSN 1016-1104

Petrogenesis of the Lalezar granitoid intrusions (Kerman Province - Iran)

S. M. Niktabar[*1], A. Moradian[1], H. Ahmadipour[1], J. F. Santos[2] and M. H. Mendes[2]

[1] *Department of Geology, Faculty of Sciences, Shahid Bahonar University of Kerman, Kerman, Islamic Republic of Iran*
[2] *Geobiotec, Department of Geosciences, University of Aveiro, 3810-193 Aveiro, Portugal*

Received: 19 August 2015 / Revised: 7 November 2015 / Accepted: 23 November 2015

Abstract

The Lalezar granitoids crop out within volcanic successions of the Urumieh-Dokhtar Magmatic Assemblage (UDMA). These granitoids have a range from gabbro-diorites to granites in composition. The mineral compositions of the most felsic rocks are characterized by the abundances of Na-plagioclase, quartz, alkali feldspar, biotite and hornblende. In the gabbro-diorite rocks, plagioclase (Ca-rich), hornblende, biotite and clinopyroxene are the most common minerals. Major element geochemical data show that the Lalezar granitoids are mostly metaluminous, although the most felsic members (granites) attain slightly peraluminous compositions and that they have features typical of high-K calc-alkaline rocks. In primitive mantle-normalized trace element spider diagrams, the analysed samples display strong enrichment in LILE compared to HFSE, accompanied by negative anomalies of Nb, Ta and Ti. REE chondrite-normalized plots show moderate LREE enrichment with slight to strong negative Eu anomalies. Rb–Sr geochronological data, mainly dependent on the Sr isotopic composition of biotite, was obtained in two samples and it points to 15-16 Ma. As a probable, age for the emplacement of the studied intrusives. Initial 87Sr/86Sr ratios and ƐNdi values range from 0.70495 to 0.70565 from +3.1 to +1.5 respectively, which fit into a supra-subduction mantle wedge source for the parental melts and indicates that, in general, crustal contribution for magma diversification was not relevant. Geochemical and isotopic evidence reveal that the Lalezar intrusions are cogenetic I-type granitoids which were generated in a continental arc setting, in agreement with models previously presented in the UDMA.

Keywords: Lalezar; Calc-alkaline; Granitoids; Petrogenesis; Isotopic composition.

Introduction

One of the most significant events in the magmatic history of Iran is a widespread magmatic flare-up that occurred mainly in the Urumieh-Dokhtar Magmatic Assemblage (UDMA), extending in the form of belt over a length of approximately 1700 km and width of about 150 km (Fig. 1(A)). This phase of magmatism is

[*] Corresponding author: Tel: +989133592860; Fax: +98343325743; Email: Maryam.Niktabar@gmail.com

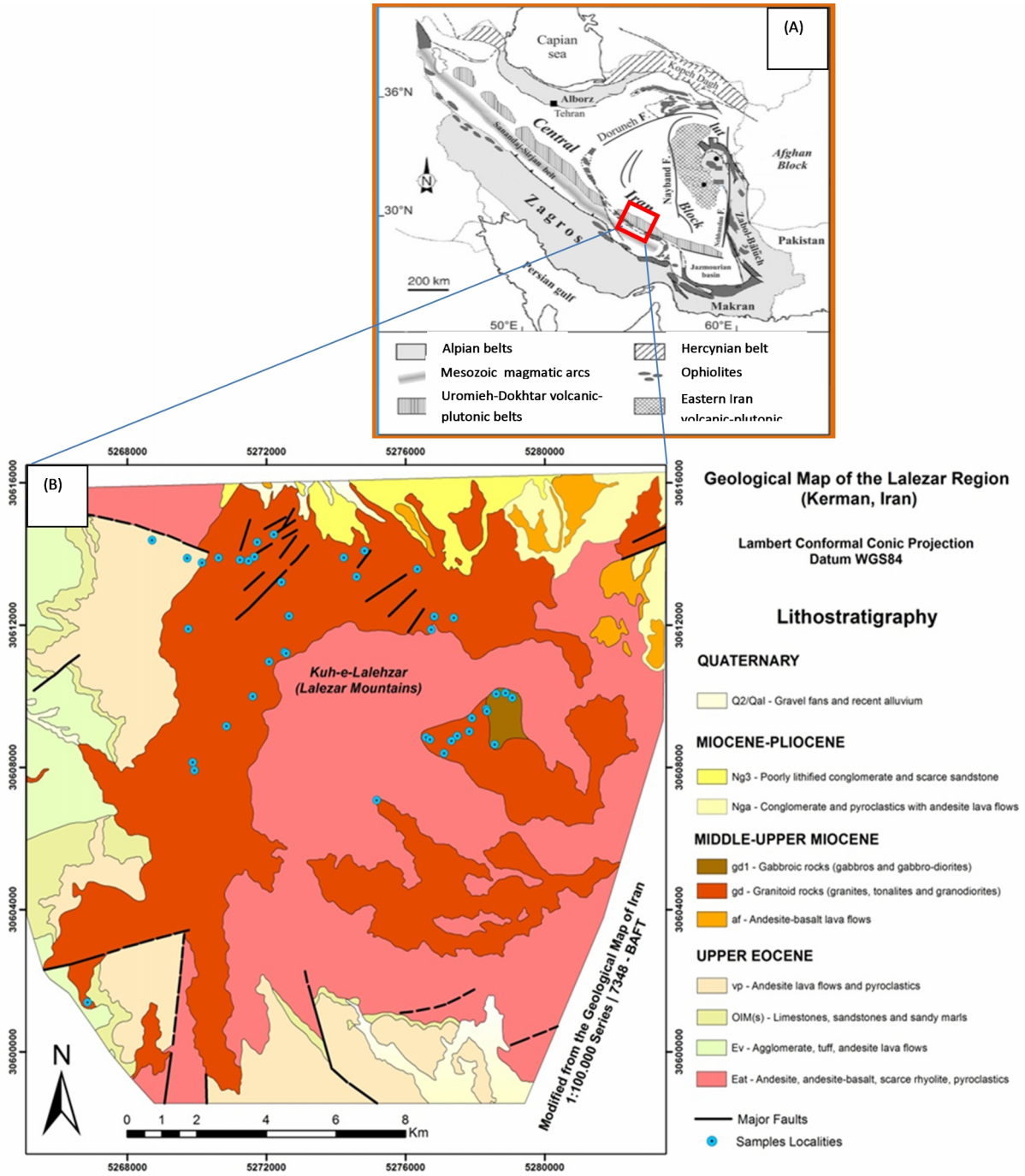

Figure 1. (A) Modified geological sketch map of Iran, after Berberian and King (1981). (B) A part of the geological map of Baft and location of the Lalezar granitoids, adapted from Srdic et al (1972).

characterized by rocks with intermediate compositions from calc-alkaline to pottasic affinity, which occur in an arc/back-arc system or extensional arc environment [1-6]; [7, 8]; [9]. However, Amidi et al. [10] represented a rift model for tectonic evolution of Eocene volcanic rocks in this belt.

Shahabpour assumes that the central Iranian volcanic belt have occurred due to the subduction of southern branches of Neothetys ocean [11]. In contrast, according to Ghasemi and Talbot [12], Eocene magmatism, is known after of the collision zone.

The UDMA contains Eocene-Quaternary intrusive

and extrusive rocks. The magmatic activity climax occurred in Eocene period [13]: [14];[15];[14];[11, 16, 17].

The Eocene magmatism presumably ceased, following the continental collision between Arabia and Eurasia [18]. The Closure of Neo-Tethyan Ocean and compression-related deformation caused shortening, crustal thickening and downward migration of the lithosphere–asthenosphere boundary, thus providing the heat and pressure required for magmatism activity [19, 20].

A part in Urumieh-Dokhtar Magmatic Assemblage (UDMA), called Dehaj-Sarduieh volcano-plutonic belt in Kerman province [21], is specified by the occurrences of numerous felsic plutons of Oligocene–Miocene age, famous for world-class porphyry copper and molybdenum deposits [22]. As a part of systematic investigations of granitoids in southwestern Kerman, authors such as Berberian and Berberian [23], [24], and [25] found that most granitoids in the area are calc-alkaline metaluminous I-type granitic to granodioritic rocks.

Concerning the fact that the mass of volcanic rocks are located in the Eocene sedimentary divisions of UDMA, the intruded bodies in volcanic-sediment rocks are possibly Oligocene-Miocene [21].

The main purpose of the current paper is to present and discuss new geochemical (both elemental and isotopic) and geochronological (Rb-Sr) data from the shallow intrusive and establish tighter constraints to the petrogenetic processes of the Lalezar granitoids.

Hence, the present contribution reports on petrographic, whole-rock geochemical, and Sm-Nd, Rb-Sr isotope characteristics of the Lalezar granitoid batholith (a probably Miocene intrusion) in the southeastern Urumieh-Dokhtar or Sahand-Bazman magmatic arc. These petrographic and geochemical data are applied to clarify the origin and tectonic evolution of granitoid batholith, particularly during the Neotethyan subduction processes.

General geology and petrography

The Lalezar granitoid masses are located in the 110 km south of Kerman, near Lalezar village, Kerman province, Iran, intruding into the lava flows and pyroclastic rocks. They cover an area of about 100 km^2. These granitoids crop out in the volcanic successions of the southeast of the Dehaj-Sarduieh volcano-plutonic belt as a part of Urumieh-Dokhtar Magmatic Assemblage (UDMA) (Fig. 1).

The Urumieh-Dokhtar Magmatic Assemblage includes alkaline and calc-alkaline volcanic rocks and the related intrusives (I-type), made by subduction of the Arabian plate beneath central Iran during Alpian orogeny [26]; [1]; [14].

The Dehaj–Sarduiyeh volcanic belt contains a broad range of Eocene volcano-sedimentary rocks, intruded by the so-called Jebale-Barez type granitoids with crystalline texture. Based on field relationships, Dimitrijevic proposed an Oligo–Miocene age for these granitoid rocks [27].

Lalezar granitoids are known as the Jebale-Barez type granitoids which intruded into the Eocene volcanic rocks [27] (Fig. 1& 2). These volcanic rocks consist of different andesit and basaltic-andesite lava flows and pyroclastics. Andesites are the most widespread rocks in most areas. There are some dark coloured low-T metamorphic rocks near intrusions. The andesites consist of hornblende, plagioclase, quartz and sometimes pyroxene phenocrysts in a fine-grained matrix. Porphyritic and sometimes trachytic textures are seen in these rocks.

This granitoid batholith is cut by a series of N-E and NE-SW trending dikes that are 1-2 m in wide and over a hundered meters in length. These dikes are mostly subvolcanic dioritic and andesitic in composition. In addition, metric-wide dikes of aplite cut through the Lalezar batholith.

The two kinds of enclaves have been recognized within the intrusive rocks: some display the same features of the andesitic host volcanic rocks, and interpreted as xenoliths; others have mineral assemblages similar to those of the enclosing granitoid but with larger proportions of mafic minerals as autolith. The enclaves of various type and size (centimeters to meters) are found through the batholith, being particularly abundant in the western and north part where they formed massive clusters.

The intrusions range from gabbrodiorite to granite, with dominance of diorite and tonalite. Dark-colored gabbrodiorite is located at the east; however, contacts between gabbrodiorite and granites are commonly not exposed.

Tonalites mostly have been emplaced in margins of the main body and containing plagioclase, quartz, hornblende and biotite, with granular to microgranular porphyritic texture (Fig. 3A). Granodiorites contain plagioclase, alkalifeldespare, quartz, hornblende, and biotite (Fig. 3B).

Diorites have gradational contact with granodiorites and contain plagioclase, pyroxene, hornblende, biotite, and less alkalifeldespare and quartz. Some pyroxene show uralitisation and have changed into amphibole (Fig. 4).

Granite rocks are generally located in east north of the body and are mainly composed of alkalifeldespar

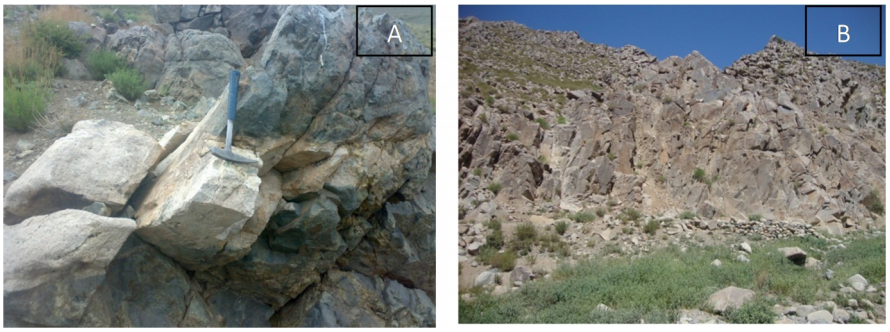

Figure 2. (A) Lalezar granitoid has intruded in volcanic rocks, (B) morphology of the granitoid.

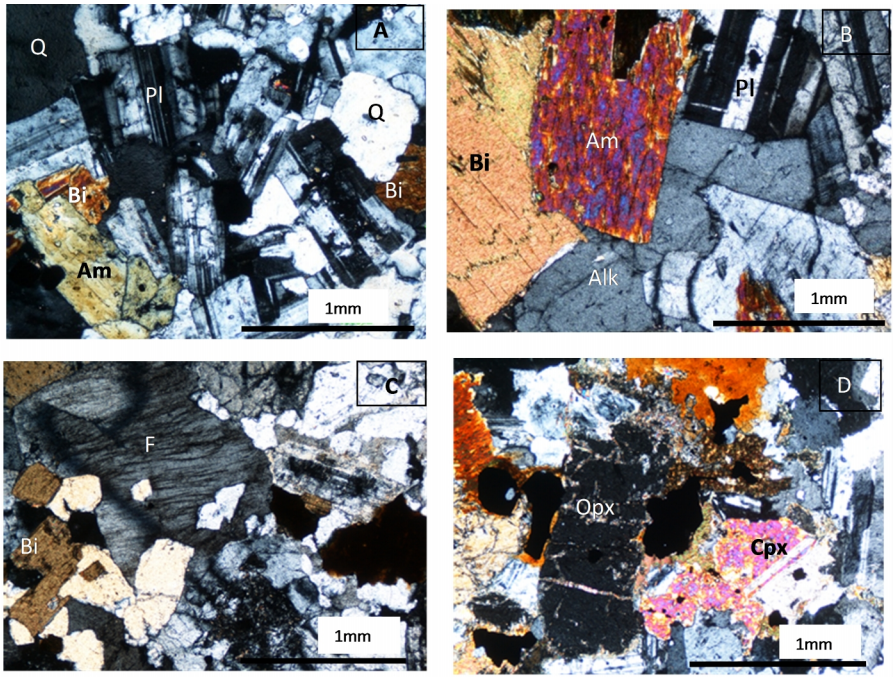

Figure 3. The mineralogical data for the rocks studied. A, Tonalite mostly consist of plagioclase and less quartz, hornblende and biotite minerals (XPL-4X). B, Granodiorite with granular texture consist of big and fresh minerals of plagioclase, alkalifeldespare, hornblende and biotite (XPL-4X). C, granite showing perthitic texture (intergrowth of a guest Na-rich plagioclase in a host K-rich feldspar) (XPL-4X) and D, gabbrodiorite with opx and cpx, some of them have altered to opaque minerals (XPL-4X).

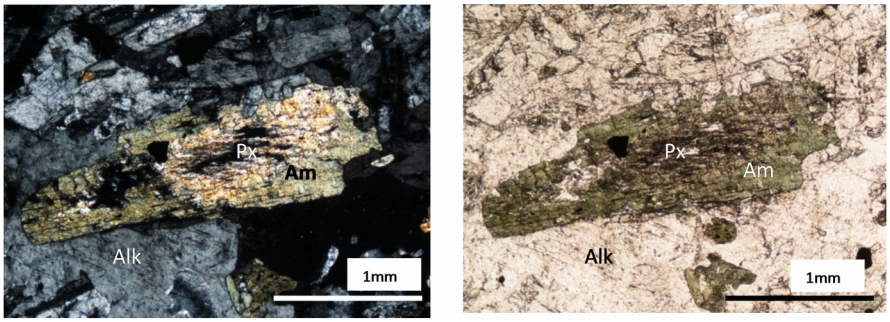

Figure 4. Pyroxene that has changed into the amphibole at its rims (XPL& PPL).

(commonly orthoclase), plagioclase, quartz, biotite and hornblende. These rocks display granular to poikilitic and perthite to granophyre texture (Fig. 3C). The granophyre is mainly composed of K-feldspar-quartz intergrowths at the eutectic point. It is crucial to note that these textures indicate that crystallization occurred

at a low temperature [28].

Gabbrodiorites in east of the body are melanocrate in appearance and are composed of plagioclase, pyroxene (cpx and opx), amphibole and rarely alkalifeldespare and quartz (Fig. 3D). Zircon, apatite, and sphene and oxide minerals are common accessory phases in these rocks.

Analytical techniques

Major and Trace element analysis after a detailed petrographic study of a large set of samples gathered from various rock units and surface exposures, 28 least altered samples were selected for whole-rock geochemical elemental analyses. Inductivity coupled plasma-mass spectrometry (ICP-MS) was applyed, followed by a lithium borate fusion and dilute acid digestion in the Acme Laboratories, Vancouver, Canada. Whole-rock analytical findings for major element oxides and trace elements are given in Table 1.

Sr and Nd isotopic compositions were determined for 14 whole-rock samples and six mineral separates (plagioclase, hornblende, and biotite from two rocks) of the Lalezar granitoids at the Laboratório de Geologia Isotópica da Universidade de Aveiro, Portugal.

The minerals were isolated from 5-ln-7 and 23-ln-6 samples by handpicking under a binocular microscope. The mineral separates were rinsed by double-distilled water and crushed several times to remove inclusions, and then ground in agate mortar. The selected powdered samples were dissolved at 200 ° C for 3 days with HF/HNO3 in Teflon Parr acid digestion bombs. The samples, after evaporation of the final solution, were dissolved with HCl (6.2 N) and dried. The target elements were purified using conventional ion chromatography technique in two stages: (1) separating Sr and REE elements in ion exchange column via AG8 50 W Bio-Rad cation exchange resin and (2) purifying Nd from other lanthanide elements in columns with Ln Resin (Eichrom Technologies) cation exchange resin. All reagents utilized in preparing the samples were sub-boiling distilled. And the water was produced by a Milli-Q Element (Millipore) apparatus. Sr was loaded on a single Ta filament with H3PO4, while Nd was loaded on a Ta outer-side filament with HCl in a triple-filament arrangement. $^{87}Sr/^{86}Sr$ and $^{143}Nd/^{144}Nd$ isotopic ratios were indicated by a Multi-Collector Thermal Ionisation Mass Spectrometer (TIMS) VG Sector 54. The data were obtained in dynamic mode with peak measurements at 1–2 V for ^{88}Sr and 0.5–1.0 V for ^{144}Nd. Sr, and Nd isotopic ratios were corrected for mass fractionation relative to $^{88}Sr/^{86}Sr$ = 0.1194 and $^{146}Nd/^{144}Nd$ = 0.7219. Average values of $^{87}Sr/^{86}Sr$= 0.710266±14 (conf. lim 95%, N=13) and $^{143}Nd/^{144}Nd$= 0.5121019±75 (conf. lim 95%, N=12) were obtained by by SRM-987 standard and JNdi-1 standard, respectively. The Rb, Sr, Sm, and Nd concentrations in the mineral separates from two rock samples (5-ln-7 and 23-ln-6) were specified by isotope dilution mass spectrometry method (IDMS), using $^{87}Rb/^{84}Sr$ and $^{150}Nd/^{149}Sm$ double spike. The Rb–Sr and Sm–Nd isotopic compositions are given in Table 2 and Table 3.

Results

Geochemistry

1. Major element geochemistry

The major and trace elements results are given as weight percent and parts per milione, respectively. Bulk major and trace elements analyses of the 28 samples from Lalezar intrusions are reported in Table 1.

Based on the scheme, the analysed samples from the Lalezar intrusive consist of three granites, four granodiorites, twelve tonalites, six diorites and three gabbrodiorites [29] (Fig. 5).

Considering K2O vs. SiO2 discrimination diagram by Peccerillo and Taylor [30], all rocks plot in the high-K calc-alkaline field (Fig. 6). Based on their mineral compositions and A/CNK <1.1 criterion [31, 32], they are known as I-type rocks, trending towards Al saturation in most evolved samples (Fig. 7).

The Harker variation diagrams show SiO2 content ranges from 55 in gabbro diorite to 72 wt% in granite (Table 1). In these diagrams, generally, there are good linear correlations between the data that are consistent with a genetic relationship between different granitoids via fractional crystallization of plagioclase, pyroxene, amphibole, oxide minerals and apatite. In Fig. 8, no

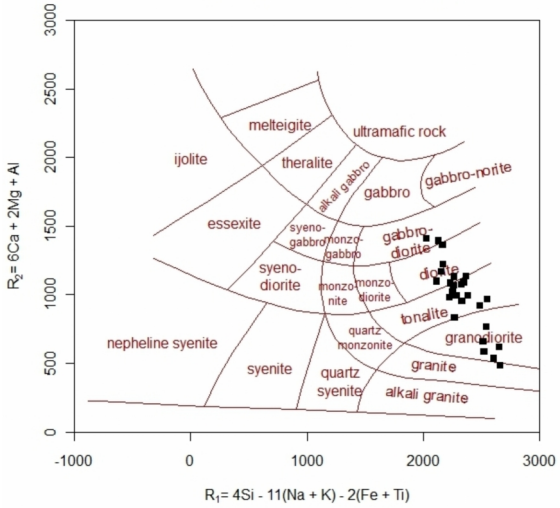

Figure 5. R1-R2 plot (De La Roche et al. 1980) diagram for the Lalezar intrusives.

Table 1. ICP Chemical analyses of the Lalezar granitoids.

Sample	7-ln-7	6-ln-2	22-ln-3	7-ln-2	8-ln-9	21-ln-16	23-ln-2
Rock	Granite	Granite	Granite	Granodiorite	Granodiorite	Granodiorite	Granodiorite
SiO2	72.78	70.29	70.6	68.96	67.07	65.47	70.74
Al2O3	13.53	14.05	13.87	14.5	15.2	15.9	14.1
Fe2O3	2.25	3.1	2.97	3.57	4.26	4.62	3.33
MgO	0.51	1.07	0.94	1.26	1.62	2.07	1.1
CaO	1.8	2.39	2.01	2.89	3.61	4.71	2.7
Na2O	2.77	2.7	3.18	2.88	2.65	3.36	2.72
K2O	4.86	4.76	3.78	4.09	3.69	2.36	4.27
TiO2	0.23	0.33	0.32	0.35	0.43	0.41	0.34
P2O5	0.05	0.07	0.07	0.08	0.08	0.1	0.07
MnO	0.04	0.06	0.04	0.04	0.05	0.11	0.05
Cr2O3	0.003	0.004	0.003	0.004	0.003	0.003	<0.002
LOI	1	1	2	1.2	1.2	0.7	0.4
Sum	99.85	99.84	99.82	99.84	99.83	99.84	99.82
Ba	505	467	571	391	449	374	470
Sc	4	7	6	7	9	11	8
Co	2.5	5.5	2.9	9.4	7	9.1	6.2
Cs	11.4	10.7	2.4	9.5	6.7	3.1	15.3
Ga	11.7	12.3	12.1	13.3	12	13.3	12.8
Hf	5.5	5.6	4.8	4.1	5.2	3.2	5.8
Nb	5.3	5.4	4.8	5.2	4	4	5.6
Rb	235.9	225.9	118.2	193.1	129.6	62.9	214.3
Sr	140	163.2	229.2	204	238.7	318.5	186.1
Ta	0.5	0.5	0.6	0.5	0.4	0.4	0.6
Th	22.6	16.5	10.2	22.2	14.5	5.5	20.4
U	5.4	4	2.5	5.6	3.4	1.2	5.5
V	24	46	43	58	71	79	52
W	2.8	1	1.3	0.7	1.4	1.2	1.4
Zr	165.7	182.4	157.9	134.2	175.8	109.4	182.7
Y	18.5	23.7	21.6	16.9	17.3	13.7	30.2
La	8.5	24.2	18.1	19	12.6	15.4	31.9
Ce	14.9	47.7	37.1	33.7	25.4	30.4	63
Pr	2.06	5.7	4.52	3.96	3	3.36	7.59
Nd	8.1	23.1	16.6	14.8	12.6	13.2	27.7
Sm	2.43	4.16	3.79	2.98	2.57	2.61	5.14
Eu	0.5	0.62	0.57	0.53	0.69	0.62	0.61
Gd	2.62	4.16	3.53	2.94	2.99	2.53	5.01
Tb	0.45	0.61	0.58	0.42	0.43	0.39	0.77
Dy	3.11	4.15	3.58	2.58	2.79	2.28	4.59
Ho	0.68	0.85	0.71	0.54	0.63	0.51	0.98
Er	1.9	2.59	2.51	1.98	1.89	1.46	3.15
Tm	0.33	0.4	0.4	0.28	0.28	0.26	0.48
Yb	2.14	2.72	2.56	1.87	1.87	1.59	3.13
Lu	0.3	0.45	0.39	0.31	0.3	0.29	0.53
Rbn/Yn	91.2776	68.2821	38.3004	81.965	53.7079	32.9103	50.8253
LaN/LuN	2.94206	5.58155	4.82164	6.36449	4.36159	5.51387	6.18557
Eu/Eu*	0.61	0.46	0.48	0.55	0.76	0.74	0.37

obvious correlation is seen between Na2O and silica contents (2.88 and 68.96, respectively), which can be due to Na metasomatism in the main intrusive body. K2O/Na2O ratios increase from 0.3 to 1.7 toward more evolved compositions. In addition, MgO, FeOt, CaO, P2O5, and TiO2 decrease with increasing SiO2 (Fig. 8). All in all, the major element variation diagrams refer to a differentiation mechanism controlled by fractionation of clinopyroxene, plagioclase, and hornblende along with crystallization order that can be inferred from textural criteria. Apatite fractionation, and to some extent oxide minerals (Fe–Ti oxides), should also have affected magma differentiation, evidenced by the constant and ongoing decreases in phosphorus, iron and titanium with increasing SiO2 contents.

The Lalezar gabbrodioritic samples have MgO contents from 3.74 to 4.23 wt%, and magnesium numbers (Mg ≠ 100 * Mg/[Mg + Fe], using atomic

Table 1. Cntd

Sample	3-ln-4	3-ln-11	8-ln-8	6-ln-8	14-ln-17	23-ln-9	23-ln-13	23-ln-14	2-ln-12	18-ln-29	5-ln-1	22-ln-14
Rock	Tonalite	Tonalite	Tonalite	Tonalite	Tonalite	Tonalite	Tonalite	Tonalite	Tonalite	Tonalite	Tonalite	Tonalite
SiO2	62.58	62.84	65.62	62.62	65.44	62.64	63.9	62.72	61.34	62.47	61.59	61.6
Al2O3	15.98	16.02	15.28	16.31	15.87	16.11	16.06	15.98	16.34	16.53	16.46	16.98
Fe2O3	6.21	6.03	4.06	5.85	4.45	5.95	5.16	5.61	6.44	5.64	6.31	6.02
MgO	2.57	2.63	1.99	2.51	2.04	2.72	2.32	2.44	2.9	2.72	2.8	2.78
CaO	5.28	5.14	4.05	5.34	5.19	5.08	4.89	5.09	5.61	5.35	5.71	5.79
Na2O	3	2.98	3.35	3.16	3.43	2.98	3.03	3.13	3.02	3.14	3.04	3.3
K2O	2.45	2.46	3.41	2.71	1.99	2.84	3.01	2.92	2.43	2.7	2.22	1.79
TiO2	0.63	0.62	0.46	0.61	0.44	0.58	0.55	0.57	0.64	0.51	0.61	0.48
P2O5	0.12	0.12	0.11	0.13	0.12	0.1	0.11	0.13	0.13	0.11	0.12	0.11
MnO	0.11	0.1	0.04	0.11	0.11	0.09	0.09	0.1	0.11	0.1	0.11	0.11
Cr2O3	0.003	0.004	0.003	0.004	0.004	0.006	0.004	0.005	0.005	0.005	0.003	0.003
LOI	0.9	0.9	1.5	0.5	0.7	0.7	0.7	1.1	0.9	0.6	0.9	0.9
Sum	99.82	99.82	99.84	99.82	99.81	99.82	99.81	99.82	99.82	99.83	99.83	99.83
Ba	342	347	372	315	491	377	397	374	327	344	284	304
Sc	16	15	10	15	11	15	14	13	18	13	18	13
Co	14.8	14.1	8.8	12.8	4.8	15.6	13.2	14.1	15.7	14.1	14.3	14.8
Cs	7	6	4.6	9.4	1.7	5.5	6.7	7.3	8.1	9.5	5.4	7
Ga	15.4	16.6	13.5	14.1	14.3	15.4	15.3	14.6	15.4	15.8	14.8	16.1
Hf	3.8	3.9	4.2	4.5	3.7	5	4.9	4.9	4.4	4.1	3.2	2.1
Nb	6.2	5.3	5.2	4.7	3.9	4.5	4.7	5	4.4	4.8	4.5	3
Rb	103.6	114.8	117.5	107.9	35	117.6	129.5	129.1	104.5	112.6	90.4	57.4
Sr	271.5	287.1	252.8	302.8	387.9	294.7	314.1	320.7	308.7	319.1	288	412.7
Ta	0.4	0.4	0.4	0.3	0.4	0.4	0.5	0.4	0.3	0.4	0.3	0.4
Th	6.6	7.4	14.7	9.9	5.8	8.6	9.9	12.9	6.9	10.2	10.1	3.7
U	1.7	2.3	3.3	2.2	0.8	2.1	2.4	3.1	1.7	2.7	1.8	0.8
V	146	132	82	116	93	121	117	118	151	109	143	126
W	1.3	2	1.6	3.3	0.7	1.2	0.9	0.9	2.8	2	4.1	2.1
Zr	130	145.5	158	170.2	118.9	167.7	167.6	175.2	144.2	124.5	102.5	82.6
Y	18.6	19.4	19.4	22.9	13.2	21.4	21.3	18.2	22.9	16.5	18	15.3
La	14.3	13.4	19.5	16.4	6.8	15.3	14.8	17	14.5	17.2	16	11.7
Ce	27.7	28	39.5	34.1	13.6	32.6	32.7	35	32.3	33.9	30.1	21.9
Pr	3.55	3.43	4.72	4.27	1.71	3.93	4.02	4.27	3.8	3.99	3.6	2.81
Nd	14	14.9	19.1	16.8	7.6	15.4	16.4	16.2	15.5	14.7	14.4	11.4
Sm	3.08	3.16	3.47	3.6	1.87	3.39	3.82	3.39	3.51	3.22	3.08	2.47
Eu	0.77	0.72	0.69	0.81	0.65	0.78	0.79	0.77	0.83	0.77	0.72	0.76
Gd	3.65	3.37	3.64	3.99	2.16	3.66	3.72	3.38	3.96	3.31	3.38	2.67
Tb	0.55	0.54	0.53	0.62	0.34	0.6	0.6	0.52	0.64	0.51	0.52	0.45
Dy	3.71	3.43	3.52	4.05	2.24	3.73	4.06	3.12	3.63	3.32	3.35	2.65
Ho	0.7	0.67	0.72	0.77	0.48	0.81	0.85	0.68	0.86	0.7	0.7	0.54
Er	2.13	2.06	2.12	2.42	1.39	2.34	2.39	2	2.52	2.03	2.05	1.72
Tm	0.33	0.29	0.33	0.35	0.23	0.34	0.35	0.29	0.39	0.34	0.32	0.26
Yb	2.17	2.04	2.32	2.44	1.58	2.23	2.44	2.01	2.47	1.96	2.04	1.79
Lu	0.33	0.33	0.33	0.36	0.26	0.32	0.33	0.33	0.37	0.32	0.31	0.28
Rbn/Yn	39.89	42.439	43.4366	33.7813	19.0069	39.4043	43.5769	50.8275	32.7177	48.8485	35.9495	26.9018
LaN/LuN	4.50049	4.21756	6.13659	4.73166	2.71871	4.96479	4.65756	5.35024	4.0705	5.58149	5.35929	4.33793
Eu/Eu*	0.7	0.67	0.59	0.65	0.99	0.68	0.64	0.7	0.68	0.72	0.68	0.9

proportions, ranging from 32.80 to 35.81. The low Mg-number, Cr and Ni contents in the mafic samples preclude their being parental melt as the mantle peridotite [33], In the other words, the parental magma of the examined rocks is not a direct partial melt of asthenospheric mantle wedge.

Phosphorus has been shown to have a profound influence on the evolution of silicate melt systems. According to diagram of P_2O_5 versus SiO_2 [34], formation temperature of Lalezar rocks can be estimated from 850 to 900 ° C (Fig. 9).

2. Trace element geochemistry

Consistent with the metaluminous and high-k and calc-alkaline features of the Lalezar granitoids, almost all samples plot in the volcanic arc granites domain in the diagrams presented by Pearce et al. [35], with a tendency toward the syn-collision granites (Fig. 10A). Fig. 10B illustrates that the Lalezar granitoids plot by and large in Syn-Collision to pre plate –Collision field

Table 1. Cntd

Sample	5-ln-7	12-ln-12	14-ln-1	18-ln-23	18-ln-26	23-ln-6	6-ln-3	17-ln-4	20-ln-11
Rock	Diorite	Diorite	Diorite	Diorite	Diorite	Diorite	Gabbrodiorite	Gabbrodiorite	Gabbrodiorite
SiO2	61.03	59.46	58.68	60.82	59.93	61.49	55.52	55.88	56.63
Al2O3	16.92	16.76	16.89	16.78	16.96	16.54	18.13	18.06	18.18
Fe2O3	6.33	7.06	7.28	6.64	7.1	5.97	7.58	7.74	7.66
MgO	2.93	3.34	3.44	3.04	2.98	2.91	4.23	4.17	3.74
CaO	6.15	6.28	6.71	6.08	5.76	5.75	7.89	7.77	7.67
Na2O	3.1	3.05	3.15	3.09	3.28	3.09	3.07	3.09	3.08
K2O	1.81	2.26	1.78	2.15	2.2	2.56	1.59	1.2	1.29
TiO2	0.6	0.72	0.75	0.66	0.63	0.58	0.68	0.73	0.68
P2O5	0.12	0.15	0.16	0.12	0.13	0.11	0.16	0.13	0.13
MnO	0.12	0.12	0.11	0.12	0.09	0.11	0.12	0.12	0.14
Cr2O3	0.002	0.005	0.005	0.003	0.003	0.005	0.005	0.006	0.003
LOI	0.7	0.6	0.9	0.3	0.7	0.7	0.8	0.9	0.6
Sum	99.83	99.83	99.83	99.82	99.81	99.82	99.81	99.84	99.82
Ba	325	307	267	306	295	307	273	206	236
Sc	15	20	20	19	16	16	20	23	23
Co	17.6	19.3	17.6	16.9	12.6	16.4	21.3	16.7	20.7
Cs	7.1	6.1	4.1	8.5	5.1	11.1	7.5	3	4.2
Ga	17.1	14.3	15	15.5	15.2	15.3	17.1	16.6	16.8
Hf	2.8	3.5	3.7	3.7	3.6	4.2	2.8	2.5	2.4
Nb	4.3	3.5	3.7	3.7	3.8	4.3	3.3	3.5	2.7
Rb	72.7	87.6	65.1	84.9	87.2	113.2	62	51.9	47.6
Sr	368.4	298.2	324.7	321.7	346.7	321.9	483.2	422.7	416.3
Ta	0.3	0.3	0.3	0.3	0.2	0.4	0.3	0.2	0.2
Th	5.4	5.7	5.5	7.5	5.5	12.4	5	4.1	3.5
U	1.2	1.3	0.8	1.4	1.4	3	1.1	0.9	0.8
V	147	160	163	162	145	139	177	189	201
W	3.3	0.7	0.8	0.9	0.5	1.3	1	0.6	1.1
Zr	90.1	120.7	105.3	123.5	117.2	147.2	108.7	85.4	79.8
Y	16.5	20.3	20.8	20.1	19	22.5	14.5	20	16.7
La	11.9	13	12.4	14.2	13.6	18.1	13.5	11.5	10.6
Ce	24.4	26.3	26.9	29.3	26.5	36.1	29.1	26	21.7
Pr	3.08	3.52	3.39	3.61	3.38	4.34	3.44	3.38	2.76
Nd	13.6	14.3	14.3	15.1	14.9	15.8	14.1	14.3	11.6
Sm	2.81	3.3	3.45	3.23	2.92	3.69	2.96	3.18	2.5
Eu	0.87	0.74	0.87	0.8	0.85	0.82	0.91	0.85	0.84
Gd	2.96	3.73	3.77	3.44	3.44	3.98	3.03	3.65	3.08
Tb	0.46	0.56	0.58	0.56	0.54	0.61	0.44	0.58	0.5
Dy	2.85	3.92	3.6	3.86	3.23	3.73	2.68	3.68	3.41
Ho	0.63	0.79	0.78	0.82	0.79	0.85	0.57	0.84	0.65
Er	1.86	2.19	2.22	2.28	2.2	2.44	1.58	2.28	1.79
Tm	0.29	0.33	0.33	0.32	0.33	0.37	0.26	0.37	0.28
Yb	1.71	2.05	2.42	2.21	2.03	2.31	1.65	2.08	1.91
Lu	0.3	0.36	0.33	0.34	0.3	0.36	0.26	0.36	0.3
Rbn/Yn	31.5399	30.9305	22.4333	30.2489	32.8517	36.0141	30.6082	18.575	15.7811
LaN/LuN	4.1191	3.71109	3.90244	4.33807	4.70708	5.22272	5.39653	3.31843	3.66845
Eu/Eu*	0.92	0.64	0.74	0.73	0.82	0.65	0.93	0.76	0.93

[36].

Primitive mantle-normalized trace element spider diagrams [37] belonging to the Lalezar intrusives show strong enrichments regarding large-ion lithophile elements (LILE) ($15.78 \leq RbN/YN \leq 81.96$) and those incompatible elements that behave as LILE (Th and U) (Fig. 12). The most characteristic high-field strength elements (HFSE), e.g., Nb,Ta, Zr, Y, Ti, and HREE, have clearly lower normalized values compared to LILE. Nb, Ta, and Ti show negative anomalies (Fig. 11). These features are specifically related to subduction-related magmas including the calc-alkaline volcanic arcs of continental active margins e.g., [38]; [39];[40]; [41]. Nb and Ta impoverishment has also been related to earlier depletion events in the mantle source rocks [42]. As Ti is concerned and the geochemical and petrographic evidence pointed above, its negative anomalies are belong to oxides' fractionation. The phosphorus negative anomalies in the studied samples are justified by apatite fractionation.

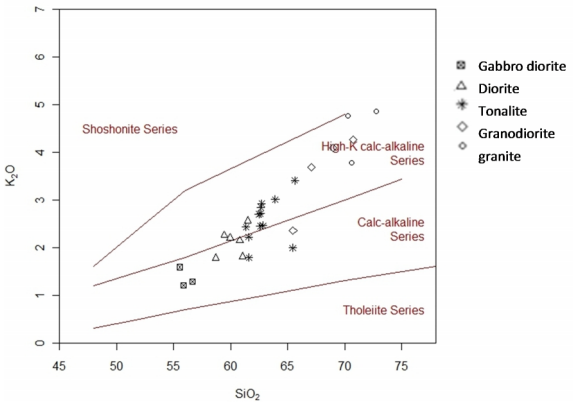

Figure 6. K2O versus SiO2 diagram. Fields after Peccerillo and Taylor (1976).

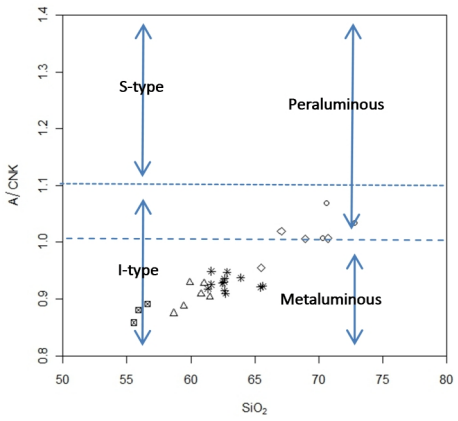

Figure 7. A/CNK versus SiO2 (Chappell and White, 1974; Chappell, 1999) for the Lalezar samples.

Rare-earth element patterns in chondrite-normalized [43] of the Lalezar intrusives are linear with a negative Eu anomaly, pointing to their cogenetic nature (Fig. 12). The REE pattern with moderate enrichment degrees for LREE ($3.32 \leq LaN/LuN \leq 6.36$) and slight to strong negative Eu anomalies ($0.46 \leq Eu/Eu^* \leq 0.92$)

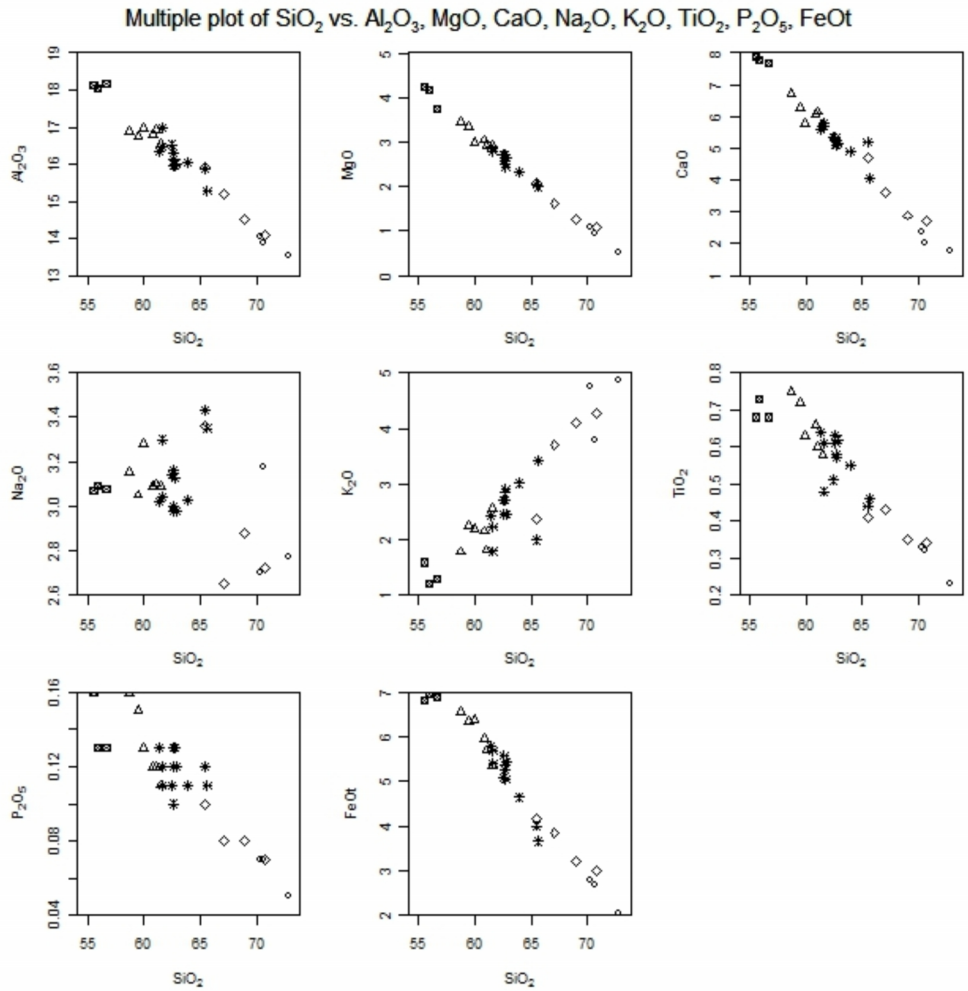

Figure 8. Variation diagrams for the intrusive rocks of Lalezar.

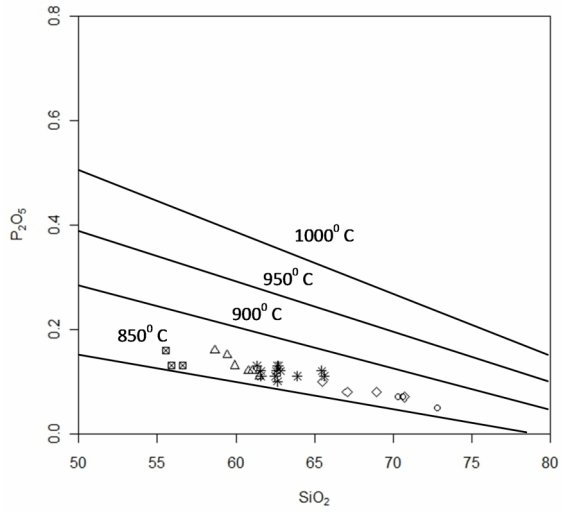

Figure 9. P2O5-SiO2 diagram for the intrusive rocks of Lalezar (Bea et al., 1992).

demonstrate high degrees of REE fractionation. Enrichment in LREE, assuming the range of LaN/YbN values between 6.0 and 2.68 (Table 1), has a flat MREE to HREE pattern. The flat HREE patterns of these rocks exclude garnet or spinel as a refractory phase while melting [44].

The Eu depletion is probably because of plagioclase removal from the source [45], or later removed by fractional crystallisation in the magma chamber prior to emplacement [46]. And it can be the result of fH2O variations during subcontinental lithosphere melting and improbable to originate from crystal fractionation [47].

Rb–Sr and Sm–Nd isotope geology

Analyses for Rb-Sr and Sm-Nd isotopic systems were obtained on fourteen whole-rock samples aiming to better constrain the petrogenetic processes responsible for the studied magma suite. Additionally, the Rb-Sr system was also used to obtain mineral – whole-rock ages in two samples. The Rb-Sr and Sm-Nd data are summarized in table 2 and table 3.

Two of the least altered samples, 5-ln-7 and 23-ln-6, were selected for Rb–Sr geochronology. Biotite (Bt), hornblende (Hbl) and plagioclase (Pl) separates were obtained from both samples. The analyses of those minerals together with results on the whole-rock (WR) samples were considered in age calculations using Isoplot 4 [48], with the ^{87}Rb decay constant proposed by Nebel and et al [49]. The results now presented are the first geochronological data for the Lalezar granitoids.

For sample 5-ln-7, using the data from the whole-rock and the three mineral separates, a $^{87}Sr/^{86}Sr$ vs.$^{87}Rb/^{86}Sr$ correlation corresponding to a 14.6 ± 5.8 Ma age is obtained, with initial $^{87}Sr/^{86}Sr$ = 0.7055 (Fig 13A). However, the MSWD has a very large value (376). This is due to the fact that Hbl composition plots deviated from the alignement defined by WR, Pl and Bt, suggesting that some disturbance took place. Under the petrographic microscope, the amphibole grains in this sample show some low temperature alteration, as testified by chloritization and oxidation, which makes plausible that a late enrichement in radiogenic Sr could have affected hornblende. If Hbl is discarded, the result now is a 15.0 ± 0.4 Ma Bt-Pl-WR isochron, with MSWD = 2.4 and initial $^{87}Sr/^{86}Sr$ = 0.70517 (Fig 13B). Considering the errors, both results (with and without

Table 2. Rb-Sr and Sm-Nd isotopic data of whole-rock samples of the Lalezar granitoids.

Sample	Rock	ppm Rb	ppm Sr	$^{87}Rb/^{86}Sr$	$^{87}Sr/^{86}Sr$	Error	ppm Sm	ppm Nd	$^{147}Sm/^{144}Nd$	$^{143}Nd/^{144}Nd$	Error	$^{87}Sr/^{86}Sr$ (T=15)	$^{143}Nd\backslash^{144}Nd$ (T=15)	€Nd (T)	TDM
6-ln-3	gabbrodiorite	62	483	0.371	0.705030	0.000018	2.50	14.1	0.127	0.512728	0.000023	0.70495	0.51271	+1.9	621
20-ln-11	gabbrodiorite	48	416	0.331	0.705030	0.000017	2.5	11.6	0.130	0.512788	0.000022	0.70496	0.51278	+3.1	544
14-ln-1	diorite	65	325	0.580	0.705158	0.000017	3.45	14.3	0.146	0.512749	0.000017	0.70504	0.51273	+2.3	733
18-ln-23	diorite	85	322	0.763	0.705403	0.000020	3.23	15.1	0.129	0.512749	0.000013	0.70524	0.51274	+2.3	602
5-ln-7	diorite	73	732	0.571	0.705278	0.000024	2.81	13.6	0.125	0.512730	0.000015	0.70516	0.51272	+1.9	604
23-ln-6	diorite	113	322	1.017	0.705481	0.000021	3.69	15.8	0.141	0.512724	0.000016	0.70529	0.51271	+1.8	737
5-ln-1	tonalite	90	288	0.908	0.705414	0.000030	3.08	14.4	0.129	0.512725	0.000015	0.70522	0.51271	+1.8	641
3-ln-4	tonalite	104	272	1.104	0.705480	0.000016	3.08	14	0.133	0.512729	0.000017	0.70525	0.51272	+1.9	661
23-ln-14	tonalite	129	321	1.164	0.705659	0.000020	3.39	16.2	0.127	0.512761	0.000019	0.70542	0.51275	+2.5	565
23-ln-13	tonalite	130	314	1.193	0.705705	0.000017	3.82	16.4	0.141	0.512746	0.000021	0.70546	0.51273	+2.2	693
21-ln-16	granodiorite	63	319	0.571	0.705089	0.000021	2.61	13.2	0.120	0.512788	0.000023	0.70497	0.51278	+3.1	486
7-ln-2	granodiorite	193	204	2.738	0.706025	0.000024	2.98	14.8	0.122	0.512705	0.000022	0.70545	0.51269	+1.5	622
6-ln-2	granite	226	163	4.004	0.706330	0.000023	4.16	23.1	0.109	0.512740	0.000015	0.70549	0.51273	+2.2	505
7-ln-7	granite	236	140	4.875	0.706667	0.000023	2.43	8.1	0.181	0.512724	0.000021	0.70565	0.51271	+1.7	1465

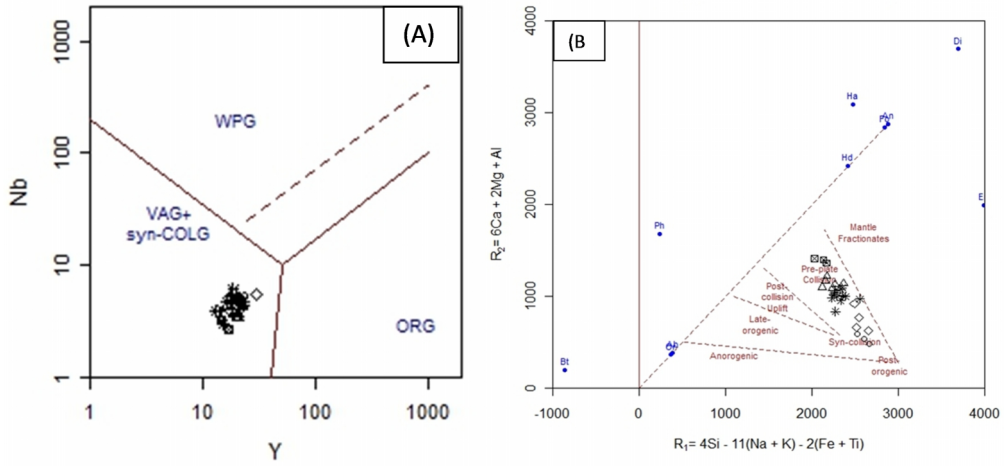

Figure 10. Tectonic discriminant diagrams for the Lalezar granitoids: (A) Y versus Nb (Pearce et al., 1984), VAG, volcanic arc granites; ORG, ocean ridge granites; WPG, within-plate granites and syn-COLG, syn-collision granites. (B) R_1 versus R_2 diagram (Bachelor and Bowden, 1985).

Hbl) overlap, which suggests that there was Sr isotope equilibrium at an age of ca. 15 Ma (most likely during igneous crystallization). The large MSWD of the Bt-Hbl-Pl-WR regression line, with Hbl plotting above that line, points to the occurrence of a post-magmatic event that affected amphibole crystals:probably, minor alteration by hydrothermal fluids with some crustal influence (higher $^{87}Sr/^{86}Sr$).

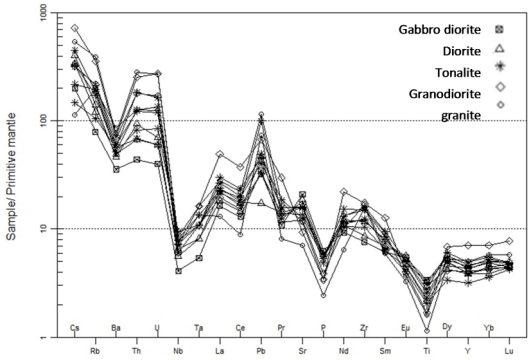

Figure 11. Primitive mantle-normalized trace element spider diagram (Sun and McDonough,1989) for the Lalezar intrusives.

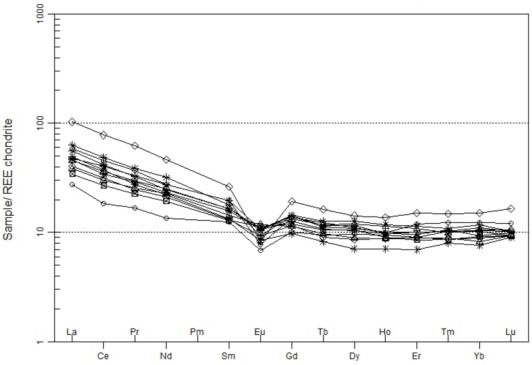

Figure 12. Chondrite-normalized diagram (Boynton, 1984) for the Lalezar intrusives.

In the $^{87}Sr/^{86}Sr$ vs. $^{87}Rb/^{86}Sr$ diagram for sample 23-ln-6, the line obtained with Bt-Hbl-Pl-WR has a slope indicating an age of 15.8 ± 1.6 Ma (Fig. 14). The MSWD value is 18 and the initial $^{87}Sr/^{86}Sr$ ratio is 0.70533. The MSWD shows that the correlation is not perfect, and, as mentioned above, it probably reflects some minor alteration; once again, Hbl plots above (slightly, in this case) the line that passes through WR, Pl and Bt. Taking the errors into account, the age calculated for 23-ln-6 overlaps the results referred for 5-ln-7 and suggests that this set of data is geochronologically meaningful. Therefore, and considering that the studied rocks are shallow intrusives which should have not undergone a long cooling period, the obtained 15-16 Ma ages are probably dating the intrusive events.

The geochronological data now presented are the first attempts to get absolute age values on the Lalezar granitoids, but previously, based on field evidence, Srdic and et al.[50] proposed an Upper-Middle Miocene age for this intrusive unit. The Rb-Sr results reported in this article fit into the lower part of the age spectrum referred by Srdic and et al.[50] and therefore, provides partial support to the conclusions presented by those authors.

Sr and Nd isotopic compositions were determined for 14 whole-rock samples. Assuming an age of 15 Ma, initial $^{87}Sr/^{86}Sr$ and ƐNdi values vary in restricted ranges between 0.70495 and 0.70565 and from +3.1 to +1.5, respectively (Table 2). In the ƐNdi versus $(^{87}Sr/^{86}Sr)i$ diagram (Fig. 15), this cluster plots to the right of the

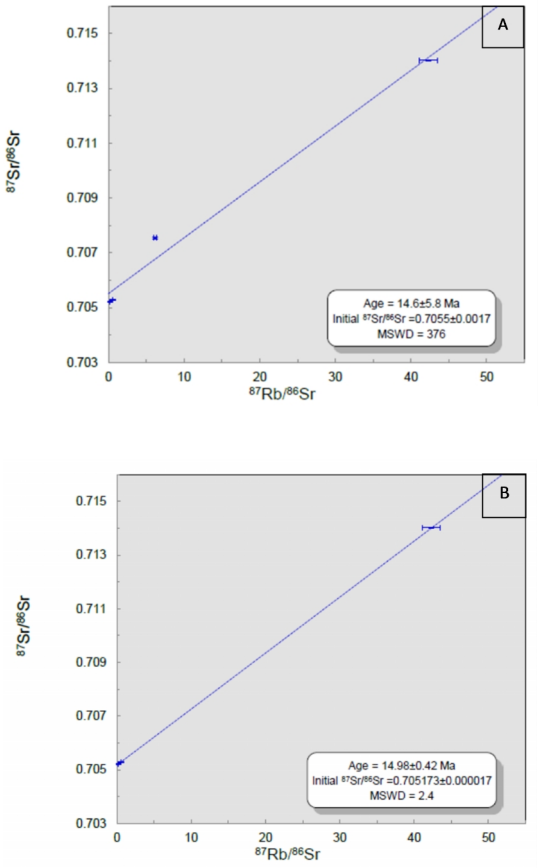

Figure 13. Plots of the Rb-Sr regression lines for sample 5-ln-7, using whole-rock and mineral compositions. (A) Using the whole-rock and the three mineral (Pl, Bt, Hlb), (B) using the whole-rock and the two mineral (Pl, Bt), without Hlb.

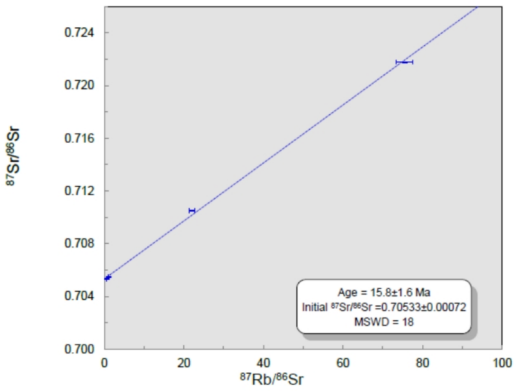

Figure 14. Plots of the Rb-Sr regression lines for sample 23-ln-6, using whole-rock and mineral compositions.

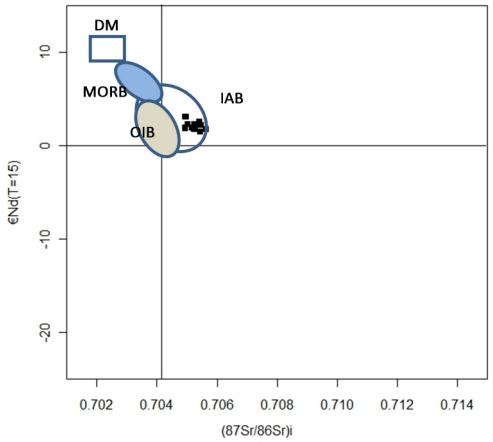

Figure 15. ƐNdi-(87Sr/86Sr)i diagram for the Lalezar intrusive rocks. MORB mid-ocean ridge basalts, DM depleted mantle, OIB ocean island basalts, IAB island-arc basalts. Initial ratios calculated for15 Ma.

so-called mantle array and overlaps the field of subduction zone.

The similar initial Sr and Nd isotopic compositions in the 14-sample cluster suggest that the Lalezar intrusions are co-genetic, deriving from the same parental magmas by magmatic differentiation processes, without significant involvement of crustal materials through processes such as mixing with anatectic melts, contamination or assimilation. Taking into account the IAB-like isotopic compositions of the studied rocks, the parental magmas may have been formed by partial melting in a supra-subduction mantle wedge [51]. The occurrence of gabbrodioritic rocks in the Lalezar suite provides additional evidence in favor of an origin of the parental magmas by melting of mantle peridotites,

Table 3. Rb-Sr isotopic data of mineral seprates from two samples (5-ln-7 and 23-ln-6) of the Lalezar granitoids (whole-rock isotopic compositions are presented in table 2).

Sample	Rock	ppm Rb	ppm Sr	$^{87}Rb/^{86}Sr$	Error	$^{87}Sr/^{86}Sr$	Error
5-ln-7-F	feldspar	30	498	0.173	0.005	0.705222	0.000024
5-ln-7-Bi	biotite	427	29	42.32	1.20	0.714020	0.000021
5-ln-7-Am	amphibole	102	48	6.19	0.175	0.707553	0.000037
Sample	Rock	ppm Rb	ppm Sr	$^{87}Rb/^{86}Sr$	Error	$^{87}Sr/^{86}Sr$	Error
23-LN-6-F	feldspar	81	410	0.6	0.01628	0.705	0.000021
23-LN-6-Bi	biotite	637	24	75.51	2.13584	0.721784	0.000036
23-LN-6-Am	amphibole	212	28	22	0.62204	0.71	0.000037

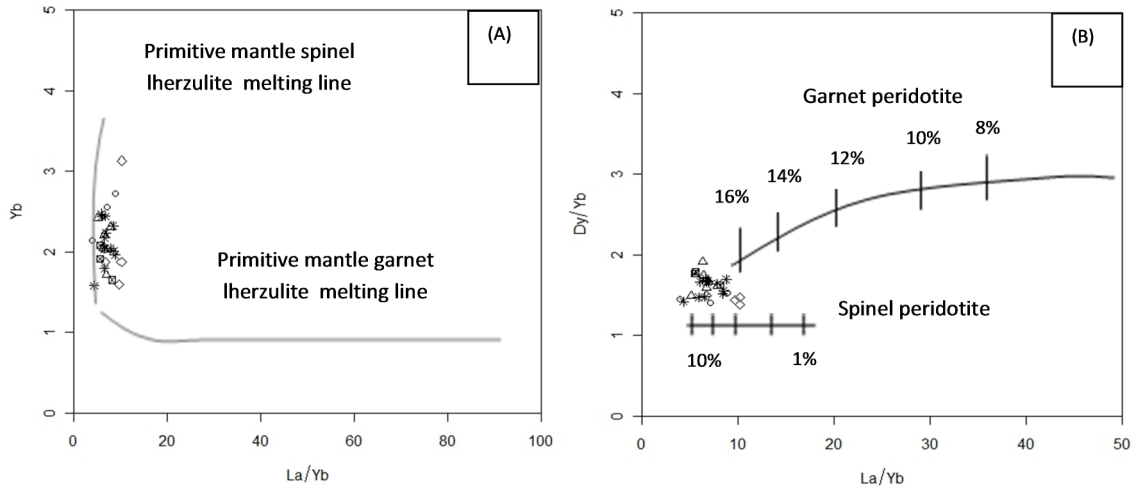

Figure 16. (A) Signification of kind of origin of studied rocks for create of magma genesis (Peters et al., 2008). (B) Signification of degree of partial melting for the origin of studied rocks (Thirwal et al., 1994).

rather than by melting of mafic crust.

In favour of the probable co-genetic nature of the studied rocks, it must be stressed that all lithologies, from the most mafic to the most felsic, have overlapping ƐNdi values. For Sr initial ratios, the variation is also small, but, in the ƐNdi vs. ($^{87}Sr/^{86}Sr$)i diagram (Fig. 15), some horizontal elongation of the cluster is observed, which suggests that the most radiogenic Sr compositions may have been variably influenced by hydrothermal fluids with crustal contribution. In fact, petrographic observations show that samples with greater initial $^{87}Sr/^{86}Sr$ values are those that underwent more intense sericitization. Since Nd is much less soluble than Sr in aqueous fluids, hydrothermal alteration may affect Sr isotopic ratio without changing the $^{143}Nd/^{144}Nd$ values.

Discussion

The chemical and the geochronological composition of the rock types in the Lalezar granitoids support the assumption that the igneous activity befell over an active subduction zone.

As shown in Fig 11, the studied rocks demonstrate obvious negative anomalies for specific elements such as Ti–Nb–Ta. The Ti–Nb–Ta negative anomalies are typical of calc-alkaline magmas, and they are interpreted by residual hornblende and/or Fe–Ti oxides in parental magmas source [52]. However, as Nb and Ta are both greatly incompatible with typical mantle assemblages and inactive during metasomatic events, their anomalies can be alternatively explained by adding slab elements to the mantle wedge from dehydrated subducted oceanic crust, increasing several incompatible elements (namely LILE), but not Nb and Ta (e.g., [53]; [54]; [55]).

Magmas rise through thickened continental crust could have been the origin of crustal contamination causing higher Rb/Sr and LILE/HFSE ratios and increasing Th contents resulting from assimilation and fractional crystallization (AFC) processes [56]. If such mechanisms had occurred extensively, significant change in Sr–Nd isotopic composition would have become apparent, and isotopic ratios' correlations with SiO2 are envisaged [57]; [58]. Restricted range of both ($^{87}Sr/^{86}Sr$)i and ƐNdi inhibits variable degrees of assimilation as a dominent process in the generation of the diverse magma compositions of the Lalezar suite, this cluster plots in the so-called mantle array and overlap the area of island-arc.

Residual garnet and amphibole may have increased the fractionation of LREE/HREE. As in works on subduction related magmatism e.g., [53], assumptions on the processes in the mantle source suffer from the fact that none of the Lalezar samples (Mg# < 35.81) and other geochemical factors exclude a direct derivation from mantle wedge. Subsequent mantle melts face and relatively re/melt the lower crustal amphibolite. As hydrous amphibolite melting produces SiO_2 rich melts [59]; [60], the resulting melts become more silicic (granitoids) compared with initial mafic intrusions (gabbros). The contribution of amphibole could have happened as low-P fractionation, and thus, its existence in the mantle source is not needed. The garnet role as a residual mantle phase is also ratios accompanied by slight HREE fractionation. Lin et al. [44] suggested that,

in some cases, melting processes in spinel peridotite sources may form magmas with LREE enrichment, but flat HREE (Fig. 12).

In Yb vs. La/Yb diagram by [61], spinel lherzolite mantle source melting may generate magma for primary parental of the granitoids (Fig. 16A). Based on La/Yb vs. Dy/Yb diagram [62], primary melts were made by10% melting of spinel peridotite in the mantle (Fig. 16B).

In the studied intrusions, magma differentiation has also been effective even on most mafic compositions and crustal contribution has not significant role in the evolution of magmas. Thus, petrogenetically, it is probable that some of primary mantle-derived melts have been generated from spinel bearing mantle peridotites in the Central Iranian Neogene subduction zone. Then they are under-plated at the arc crustal base and generated the Lalezar parental magmas by magmatic fractionation processes without significant involvement of crustal materials through processes such as mixing with anatectic melts, contamination or assimilation in crustal magmatic chambers.

It has been considered that the studied rocks are shallow intrusives which should have not undergone a long cooling period (formation temperature of Lalezar rocks can be 850 to 900℃ (Fig. 9)).

Conclusion

Lalezar granitoids intruded into the Eocene volcano-sedimentary rocks. And their compositions range from gabbrodiorites to granites, diorites and tonalites dominating. The mineral composition of the most felsic rocks is featured by the high amount of Na-plagioclase, quartz, alkali feldspar, biotite and hornblende in granodiorites and tonalites. In dioritic and gabbrodioritic rocks, the most common minerals are plagioclase (Ca-rich, in the most mafic lithologies), hornblende, biotite, clinopyroxene and orthopyroxene.

The petrographical geochemical features of the rock types in the Lalezar granitoids support the assumption that they have characteristics typical of metaluminus, I-type and Calc-alkaline rocks above an active subduction zone, consistent with models presented before to the UDMA.

Generally, Harker diagrams represent adequate linear correlations in line with a genetic relationship between different granitoids, via fractional crystallization of plagioclase, pyroxene, amphibole, oxide minerals and apatite.

In primitive mantle-normalized trace element spider diagrams, the analyzed samples show strong enrichment in LILE compared with HFSE, accompanied by Nb, Ta and Ti negative anomalies. These characteristics are related to subduction- related magmas. REE chondrite-normalized plots show moderate LREE and flat MREE to HREE pattern with linear pattern, representing their cogenetic nature.

Isotope geochemistry suggests that the studied rocks are co-genetic and are interrelated by magmatic differentiation processes such as fractional crystallization without extensive crustal contamination. The Sr–Nd isotope ratios connote high $^{143}Nd/^{144}Nd$ (0.51270– 0.51277) ratios and low $^{87}Sr/^{86}Sr$ (0.70503–0.70666) initial ratios, hence, a positive ƐNdi (1.46–3.08), confirming that the Lalezar granitoids come from the mantle over the subduction zone. The Rb-Sr dating shows the granitoids emplacement in the Miocene (15-16Ma).

The isotope ratios and the chemical composition do not acknowledge a crustal origin for the Lalezar granitoids. Our results in this paper clarify that the Lalezar granitoids are highly similar to those of normal island-arc magmas, referring to melting in a mantle wedge followed by magmatic differentiation and formation of Lalezar rocks between 850 to 900℃. Probably, metasomatism and melting processes in spinel peridotite source may form magmas for granitoides' parental in a supra-subduction mantle wedge.

Acknowledgments

The authors wish to thank Mrs. Sara Ribeiro (Laboratório de Geologia Isotópica da Universidade de Aveiro) for the TIMS analysis and for the guidance and assistance during sample preparation in the clean room. António Silva, also from Universidade de Aveiro, is acknowledged by his precious help in the adaptation of the geological map of the Lalezar area. Analyses for Rb-Sr and Sm-Nd isotopic systems were financially supported by the Geobiotec Research Unit (UID/GEO/04035/2013) funded by the Portuguese Foundation for Science and Technology. Ministry of Sciences, Research, and Technology of Iran is thanked for financial support to other components of this work, and, in particular, to the expenses for sabbatical leave of Sayedeh Maryam Niktabar in Portugal. Mohammad Noorizade is acknowledged for cooperation in the field work.

References

1. Berberian M. The southern Caspian: a compressional depression floored by a trapped, modified oceanic crust. *CaJES* **20**: 163-183 (1983).
2. Hassanzadeh J., Axen G.J., Guest B., Stockli D.F. and Ghazi A.M. presented at the 2004 Denver Annual

Meeting, 2004 (unpublished).
3. Allen M., Ghassemi M., Shahrabi M. and Qorashi M. Accommodation of late Cenozoic oblique shortening in the Alborz range, northern Iran. *JSG* **25**: 659-672 (2003).
4. Allen M.B., Vincent S.J., Alsop G.I., Ismail-zadeh A. and Flecker R. Late Cenozoic deformation in the South Caspian region: effects of a rigid basement block within a collision zone. *Tectp* **366**: 223-239 (2003).
5. McQuarrie N., Stock J., Verdel C. and Wernicke B. Cenozoic evolution of Neotethys and implications for the causes of plate motions. *GeoRL* **30** (2003).
6. Vincent S.J., Allen M.B., Ismail-Zadeh A.D., Flecker R., Foland K.A. and Simmons M.D. Insights from the Talysh of Azerbaijan into the Paleogene evolution of the South Caspian region. *GSAMB* **117**: 1513-1533 (2005).
7. Agard P., Omrani J., Jolivet L., Whitechurch H., Vrielynck B., Spakman W., Monié P., Meyer B. and Wortel R. Zagros orogeny: a subduction-dominated process. *GeoM* **148**: 692-725 (2011).
8. Verdel C., Wernicke B.P., Hassanzadeh J. and Guest B. A Paleogene extensional arc flare-up in Iran. *Tecto* **30** (2011).
9. Allen M., Kheirkhah M., Neill I., Emami M. and McLeod C. Generation of arc and within-plate chemical signatures in collision zone magmatism: Quaternary lavas from Kurdistan Province, Iran. *JPet* **54**: 887-911 (2013).
10. Amidi S.M., Emami M.H. and Michel R. Alkaline character of Eocene volcanism in the middle part of Central Iran and its geodynamic situation. *Geologische Rundschau* **73**: 917-932 (1984).
11. Shahabpour J. Tectonic evolution of the orogenic belt in the region located between Kerman and Neyriz. *JAESc* **24**: 405-417 (2005).
12. Ghasemi A. and Talbot C.J. A new tectonic scenario for the Sanandaj–Sirjan Zone (Iran). *JAESc* **26**: 683-693 (2006).
13. Stöcklin J. Northern Iran: Alborz Mountains. *Geological Society, London, Special Publications* **4**: 213-234 (1974).
14. Berberian M. and King G. Towards a paleogeography and tectonic evolution of Iran. *CaJES* **18**: 210-265 (1981).
15. Forster H., Fesefeldt K. and Kursten M. presented at the 24th International Geology Congress, Section, 1972 (unpublished).
16. Hassanzadeh J. University of California, Los Angeles, 1993.
17. Mohajjel M., Fergusson C. and Sahandi M. Cretaceous–Tertiary convergence and continental collision, Sanandaj–Sirjan zone, western Iran. *JAESc* **21**: 397-412 (2003).
18. Allen M.B. and Armstrong H.A. Arabia–Eurasia collision and the forcing of mid-Cenozoic global cooling. *Palaeogeography, Palaeoclimatology, Palaeoecology* **265**: 52-58 (2008).
19. Mirnejad H., Hassanzadeh J., Cousens B. and Taylor B. Geochemical evidence for deep mantle melting and lithospheric delamination as the origin of the inland Damavand volcanic rocks of northern Iran. *JVGR* **198**: 288-296 (2010).
20. Maghdour-Mashhour R., Esmaeily D., Shabani A.A.T., Chiaradia M. and Latypov R. Petrology and geochemistry of the Karaj Dam basement sill: Implications for geodynamic evolution of the Alborz magmatic belt. *Chemie der Erde-Geochemistry* (2015).
21. Dimitrijevic M.D. *Geology of Kerman region*. (Inst. for Geological and Mining Exploration and Investigation of Nuclear and other Mineral Raw Materials, 1973).
22. Taghipour N., Aftabi A. and Mathur, R. Geology and Re-Os Geochronology of Mineralization of the Miduk Porphyry Copper Deposit, Iran. *Resource Geology* **58**: 143-160 (2008).
23. Berberian F. and Berberian M. Tectono-plutonic episodes in Iran. *Zagros Hindu Kush Himalaya Geodynamic Evolution*: 5-32 (1981).
24. Berberian F., Muir I., Pankhurst R. and Berberian M. Late Cretaceous and early Miocene Andean-type plutonic activity in northern Makran and Central Iran. *Journal of the Geological Society* **139**: 605-614 (1982).
25. Dargahi S. Post-collisional Miocene magmatism in the Sarcheshmeh-Shahrebabak region NW of Kerman: Isotopic study, petrogenetic analysis and geodynamic pattern of granitoid intrusives and the role of adakitic magmatism in development of copper minralization. *Unpublished Ph. D. thesis, Shahid Bahonar University of Kerman* **310** (2007).
26. Stöcklin J. and Setudinia A. Lexique Stratigraphique International Volume III ASIE. *Centre National de la Recherche Scientifique* **15** (1972).
27. Dimitrijevic M. Geology of Kerman region.(Iran Geological Survey Report No. Yu/52.) Institute for Geological and Mining Exploration and Institution of Nuclear and Other Mineral Raw Materials. *Beograd Yugoslavia, p334* (1973).
28. Watson E.B. and Harrison T.M. Zircon saturation revisited: temperature and composition effects in a variety of crustal magma types. *Earth. Planet. Sci. Lett.* **64**: 295-304 (1983).
29. De La Roche H., Leterrier J., Grandclaude P. and Marchal M. A classification of volcanic and plutonic rocks using R_1 R_2-diagram and major-element analyses—Its relationsps with current nomenclature. *Chem. Geol.* **29**: 183-210 (1980).
30. Peccerillo A. and Taylor S.R. Geochemistry of Eocene calc-alkaline volcanic rocks from the Kastamonu area, northern Turkey. *Contrib. Mineral. Petrol.* **58**: 63-81 (1976).
31. Chappell B. and White A.J.R. Two contrasting granite types: 25 years later. *Australian Journal of Earth Sciences* **48**: 489-499 (2001).
32. Chappell B. Aluminium saturation in I-and S-type granites and the characterization of fractionated haplogranites. *Litho* **46**: 535-551 (1999).
33. Seymour K.S. and Vlassopoulos D. The potential for future explosive volcanism associated with dome growth at Nisyros, Aegean volcanic arc, Greece. *JVGR* **37**: 351-364 (1989).
34. Bea F., Fershtater G. and Corretgé L.G. The geochemistry of phosphorus in granite rocks and the effect of aluminium. *Litho* **29**: 43-56 (1992).
35. Pearce J.A., Harris N.B. and Tindle A.G. Trace element discrimination diagrams for the tectonic interpretation of granitic rocks. *JPet* **25**: 956-983 (1984).
36. Batchelor R.A. and Bowden P. Petrogenetic interpretation of granitoid rock series using multicationic parameters.

Chem. Geol. **48**: 43-55 (1985).
37. Sun S.S., McDonough W.F. Chemical and isotopic systematics of oceanic basalts: implications for mantle composition and processes. Geol Soc SP **42**:313–345 (1989).
38. Gill J.B. *Orogenic andesites and plate tectonics*. (Springer-Verlag Berlin, 1981).
39. Pearce J.A. Role of the sub-continental lithosphere in magma genesis at active continental margins. (1983).
40. Wilson B.M. *Igneous petrogenesis a global tectonic approach*. (Springer, 1989).
41. Walker J.A., Patino L.C., Carr M.J. and Feigenson M.D. Slab control over HFSE depletions in central Nicaragua. *Earth. Planet. Sci. Lett.* **192**: 533-543 (2001).
42. Woodhead J., Eggins S. and Gamble J. High field strength and transition element systematics in island arc and back-arc basin basalts: evidence for multi-phase melt extraction and a depleted mantle wedge. *Earth. Planet. Sci. Lett.* **114**: 491-504 (1993).
43. Boynton W.V. Geochemistry of the rare earth elements: meteorite studies. In: Henderson P (ed) Rare earth element geochemistry. Elsevier, Amsterdam, pp 63–114 (1984).
44. Lin P.N., Stern R.J. and Bloomer S.H. Shoshonitic volcanism in the Northern Mariana Arc: 2. Large-ion lithophile and rare earth element abundances: Evidence for the source of incompatible element enrichments in intraoceanic arcs. Journal of Geophysical Research: Solid Earth (1978–2012) 94: 4497-4514 (1989).
45. Clarke D.B. Granitoid rocks. (Springer, 1992).
46. Emmermann R.t., Daieva L. and Schneider J. Petrologic significance of rare earths distribution in granites. Contrib. Mineral. Petrol. 52: 267-283 (1975).
47. Tepper J.H., Nelson B.K., Bergantz G.W. and Irving A.J. Petrology of the Chilliwack batholith, North Cascades, Washington: generation of calc-alkaline granitoids by melting of mafic lower crust with variable water fugacity. *Contrib. Mineral. Petrol.* **113**: 333-351 (1993).
48. Ludwig K.R. (Berkeley Geochronology Center Special. 75 (2012).
49. Nebel O., Scherer E.E. and Mezger K., Evaluation of the 87Rb decay constant by age comparison against the U–Pb system. *Earth. Planet. Sci. Lett.* **301**: 1-8 (2011).
50. Srdic A., Dimitrijevic M.N., Cvetic S.a. and Dimitrijevic M.D. (Geological Survey of Iran, Tehran, 1972), pp. Offset Press Incorporated.
51. Stolz A., Jochum K., Spettel B. and Hofmann A. Fluid- and melt-related enrichment in the subarc mantle: evidence from Nb/Ta variations in island-arc basalts. *Geo* **24**: 587-590 (1996).
52. Pearce J.A. and Norry M.J. Petrogenetic implications of Ti, Zr, Y, and Nb variations in volcanic rocks. *Contrib. Mineral. Petrol.* **69**: 33-47 (1979).
53. Turner S., Foden J., George R., Evans P., Varne R., Elburg M. and Jenner G. Rates and processes of potassic magma evolution beneath Sangeang Api volcano, East Sunda arc, Indonesia. *JPet* **44**: 491-515 (2003).
54. Wang Q., Wyman D.A., Xu J.-F., Zhao Z.-H., Jian P., Xiong X.-L., Bao Z.-W., Li C.-F. and Bai Z.-H. Petrogenesis of Cretaceous adakitic and shoshonitic igneous rocks in the Luzong area, Anhui Province (eastern China): implications for geodynamics and Cu–Au mineralization. *Litho* **89**: 424-446 (2006).
55. Tamura Y., Ishizuka O., Stern R., Shukuno H., Kawabata H., Embley R., Hirahara Y., Chang Q., Kimura J.-I. and Tatsumi Y. Two primary basalt magma types from northwest Rota-1 volcano, Mariana arc and its mantle diapir or mantle wedge plume. *JPet*: egr022 (2011).
56. Esperança S., Crisci G.M., De Rosa R. and Mazzuoli R. The role of the crust in the magmatic evolution of the island of Lipari (Aeolian Islands, Italy). *Contrib. Mineral. Petrol.* **112**: 450-462 (1992).
57. Castillo P.R., Janney P.E. and Solidum R.U. Petrology and geochemistry of Camiguin Island, southern Philippines: insights to the source of adakites and other lavas in a complex arc setting. *Contrib. Mineral. Petrol.* **134**: 33-51 (1999).
58. Arjmandzadeh R. and Santos J. Sr–Nd isotope geochemistry and tectonomagmatic setting of the Dehsalm Cu–Mo porphyry mineralizing intrusives from Lut Block, eastern Iran. *IJEaS* **103**: 123-140 (2014).
59. Sen C. and Dunn T. Dehydration melting of a basaltic composition amphibolite at 1.5 and 2.0 GPa: implications for the origin of adakites. *Contrib. Mineral. Petrol* **117**: 394-409 (1994).
60. Rushmer T. Partial melting of two amphibolites: contrasting experimental results under fluid-absent conditions. *Contrib. Mineral. Petrol.* **107**: 41-59 (1991).
61. Peters T.J., Menzies M., Thirlwall M. and Kyle P.R. Zuni–Bandera volcanism, Rio Grande, USA—Melt formation in garnet-and spinel-facies mantle straddling the asthenosphere–lithosphere boundary. *Litho* **102**: 295-315 (2008).
62. Thirlwall M., Upton B. and Jenkins C. Interaction between continental lithosphere and the Iceland plume—Sr-Nd-Pb isotope geochemistry of Tertiary basalts, NE Greenland. *JPet* **35**: 839-879 (1994).